UDC 621.3 https://doi.org/10.20998/2074-272X.2023.1.09

Ch. Sathish, I.A. Chidambaram, M. Manikandan

Intelligent cascaded adaptive neuro fuzzy interface system controller fed KY converter for hybrid energy based microgrid applications

Purpose. *This article proposes a new control strategy for KY (DC-DC voltage step up) converter. The proposed hybrid energy system fed KY converter is utilized along with adaptive neuro fuzzy interface system controller. Renewable energy sources have recently acquired immense significance as a result of rising demand for electricity, rapid fossil fuel exhaustion and the threat of global warming. However, due to their inherent intermittency, these sources offer low system reliability. So, a hybrid energy system that encompasses wind/photovoltaic/battery is implemented in order to obtain a stable and reliable microgrid. Both solar and wind energy is easily accessible with huge untapped potential and together they account for more than 60 % of yearly net new electricity generation capacity additions around the world.* ***Novelty.*** *A KY converter is adopted here for enhancing the output of the photovoltaic system and its operation is controlled with the help of a cascaded an adaptive neuro fuzzy interface system controller.* ***Originality.*** *Increase of the overall system stability and reliability using hybrid energy system fed KY converter is utilized along with adaptive neuro fuzzy interface system controller.* ***Practical value.*** *A proportional integral controller is used in the doubly fed induction generator based wind energy conversion system for controlling the operation of the pulse width modulation rectifier in order to deliver a controlled DC output voltage. A battery energy storage system, which uses a battery converter to be connected to the DC link, stores the excess power generated from the renewable energy sources. Based on the battery's state of charge, its charging and discharging operation is controlled using a proportional integral controller. The controlled DC link voltage is fed to the three phase voltage source inverter for effective DC to AC voltage conversion. The inverter is connected to the three phase grid via an LC filter for effective harmonics mitigation. A proportional integral controller is used for achieving effective grid voltage synchronization.* ***Results.*** *The proposed model is simulated using MATLAB/Simulink, and from the obtained outcomes, it is noted that the cascaded adaptive neuro fuzzy interface system controller assisted KY converter is capable of maintaining the stable operation of the microgrid with an excellent efficiency of 93 %.* References 21, table 1, figures 20.

Key words: **photovoltaic system, hybrid energy system, proportional integral controller, adaptive neuro fuzzy interface system controller.**

Мета*. У цій статті пропонується нова стратегія управління перетворювачем КУ (підвищення напруги постійного струму). Пропонована гібридна енергетична система, що живиться перетворювачем КУ, використовується разом із контролером системи адаптивного нейро-нечіткого інтерфейсу. Відновлювані джерела енергії останнім часом набули величезного значення внаслідок зростання попиту на електроенергію, швидкого виснаження викопного палива та загрози глобального потепління. Однак через властиву їм уривчастість ці джерела забезпечують низьку надійність системи. Таким чином, гібридна енергетична система, що включає енергію вітру/фотоелектричних елементів/акумулятору, реалізована для отримання стабільної і надійної мікромережі. Як сонячна, так і вітрова енергія доступні з величезним невикористаним потенціалом, і разом вони забезпечують понад 60 % щорічного чистого приросту нових потужностей з виробництва електроенергії в усьому світі.* ***Новизна****. Перетворювач КУ використовується тут для підвищення вихідної потужності фотоелектричної системи, і його робота керується за допомогою каскадного контролера системи з адаптивним нейро-нечітким інтерфейсом.* ***Оригінальність****. Підвищення загальної стабільності та надійності системи за допомогою гібридної енергетичної системи, що живиться перетворювачем КУ і використовується разом з контролером системи з адаптивним нейро-нечітким інтерфейсом.* ***Практична цінність****. Пропорційний інтегральний контролер використовується в системі перетворення енергії вітру на основі асинхронного генератора з подвійним живленням для управління випрямлячою роботою з широтно-імпульсною модуляцією для забезпечення регульованої вихідної напруги постійного струму. Акумуляторна система накопичення енергії, в якій використовується акумуляторний перетворювач для підключення до кола постійного струму, зберігає надмірну потужність, що виробляється з відновлюваних джерел енергії. Залежно від стану заряду акумулятора, процес його зарядки і розрядки контролюється за допомогою пропорційного інтегрального контролера. Керована напруга кола постійного струму подається на трифазний інвертор джерела напруги для ефективного перетворення постійної напруги змінну. Інвертор підключений до трифазної мережі через LC-фільтр для ефективного придушення гармонік. Пропорційний інтегральний регулятор використовується для досягнення ефективної синхронізації напруги мережі.* ***Результати****. Запропонована модель змодельована з використанням MATLAB/Simulink, і з отриманих результатів випливає, що каскадний адаптивний нейро-нечіткий інтерфейс із системним контролером та перетворювачем КУ здатний підтримувати стабільну роботу мікромережі з чудовим ККД 93 %.* Бібл. 21, табл. 1, рис. 20.

Ключові слова: **фотогальванічна система, гібридна енергетична система, пропорційний інтегральний контролер, системний контролер з адаптивним нейро-нечітким інтерфейсом.**

Introduction. The increasing energy demand and awareness about the harmful consequences of carbon emissions from fossil fuels have intensified the need for infusion of clean and sustainable sources of energy that includes wind, solar, biomass and fuel cell into electrical systems. Among these, solar and wind power, in particular have grown at an incredible rate during the last decade. Since, both are non-polluting, abundantly available and generate power closer to load centers [1]. The widespread integration of renewable energy sources (RESs) into the utility AC grid causes voltage fluctuations and protection issues [2]. As a result, the utility grid's reliability, security and quality are highly affected. To subdue the effect of these issues, a new concept called microgrid has been developed for future electrical power systems. Microgrid is an interconnected network of Distributed sources of energy, loads and energy storage systems (ESS) that operates in either grid connected mode or islanded mode [3, 4]. Microgrids are basically categorized as AC, DC and hybrid microgrid on the basis of the voltages and currents used [5]. The voltage output from a photovoltaic (PV) is basically a low DC voltage and it fluctuates with the varying weather conditions and solar irradiance, hence a DC-DC converter is considered to be crucial for the conversion of the low voltage to a

high voltage [6]. Different DC-DC converters like boost [7], buck-boost [8], Cuk [9], SEPIC [10] and so on are used with the PV system for the purpose of executing effective DC-DC conversion process.

By using efficient control techniques, the efficiency of the converter is significantly improved with the reduction of total harmonic distortion, settling time, peak overshoot issues and steady state error. The control techniques are categorized into two major types, which are conventional control and intelligent control [11]. The conventional control technique like PI controller is simple in design and effectively controls the DC quantities. However, this controller suffers from certain drawbacks like nonzero steady state error, poor performance during sudden load variations and excessive integration of distributed energy resources in microgrid. Additionally, for the system's operation, an accurate mathematical model is required. Artificial neural network (ANN), fuzzy logic controller (FLC), and neuro fuzzy systems are examples of intelligent control approaches. When compared to conventional PI controller, these techniques are more reliable and efficient as they enhance a system's dynamic performance without the requirement of an accurate mathematical model of the system. One of the most frequently used approach in microprocessor-based control system is FLC because its working is not affected by the fluctuations in operating points and PV parameters. However, it is an error prone and time-consuming approach as it works on the basis of membership functions and rule base. ANN, which is made up of a group of simple processing interconnected neurons, replicates the human learning approach. Here, the learning process is complicated and focused on a number of methods. Moreover, it is too difficult to create a mathematical model that incorporates all of these methods. The adaptive network based fuzzy inference system (ANFIS) is a neuro fuzzy system that combines ANN and FLC characteristics. Here, the parameters and structure of a fuzzy inference system are identified and tuned using neural learning rules solely with the given data [12-15].

In [16], both doubly fed induction generator (DFIG) based wind energy conversion system (WECS) and solar PV system are integrated into the microgrid for providing seamless power supply. The two most common types of wind turbines utilised for wind energy extraction are variable-speed and fixed-speed wind turbines. Fixed speed wind turbines are simple in operation, but generation of high-power losses has limited their application. Variable-speed wind turbines with DFIG are broadly utilized due to the several advantages they provide, including lower acoustic noise, lower converter ratings, excellent energy efficiency and minimum power loss.

The stability, resiliency and efficiency of the electric power grid are greatly improved by using a proper ESS. Some of the most essential tasks of the ESSs are to store the surplus energy generated from the RESs, to smoothen the variations that result from the non-linear quality of the RES, to heighten the flexibility and security of the power system [17-19]. For the sake of minimizing the DC voltage fluctuations, a bidirectional DC-DC converter is implemented for interfacing the ESS to the DC bus [20, 21].

A hybrid wind/PV/battery based microgrid is designed in this research work. The non-linear output from the PV is stabilized using cascaded ANFIS assisted KY converter (KY is the name given to this converter by the first letters of both authors **K**.I. Haw, **Y**.T. You). The output from the DFIG based WECS is stabilized using PI controller. The excess power from both PV and WECS is stored in battery energy storage system (BESS), which acts as a secondary power source in the absence of power supply from primary sources. The interfacing of battery to the microgrid is accomplished using a battery converter and the state of charge (SOC) of the battery is managed using a PI controller. The effective grid synchronisation is also achieved by the control of 3φ voltage source inverter (VSI) using the PI controller. The performance of the designed hybrid microgrid in enhancing the voltage stability is examined using MATLAB simulations.

Proposed system description. The PV system's output is generally low, so a KY converter is implemented for boosting the solar panels output voltage. The output of the converter is not stable and experience incessant fluctuations due to the intermittency of the PV system so the cascaded ANFIS controller is chosen for stabilizing the converter output. The error signal obtained by comparing the actual DC voltage output $V_{DC_{act}}$ of the converter to the reference voltage $V_{DC_{ref}}$ is fed to cascaded ANFIS controller. The reference signal generated from the controller is provided to the PWM generator for the purpose of generating PWM pulses. The resultant pulses control the switching action of the converter so as to produce a stable output. Figure 1 illustrates the block diagram of proposed hybrid energy based microgrid. In the WECS, the wind turbine produces mechanical energy by conversion of the kinetic energy of the wind, whereas the DFIG produces electrical energy by conversion of mechanical energy. The obtained electrical energy is AC, hence the conversion of AC voltage to DC voltage is carried out using a pulse width modulation (PWM) rectifier. The output power of the WECS fluctuates with the changing wind speed, so the PI controller is used for stabilizing the voltage output of the PWM rectifier.

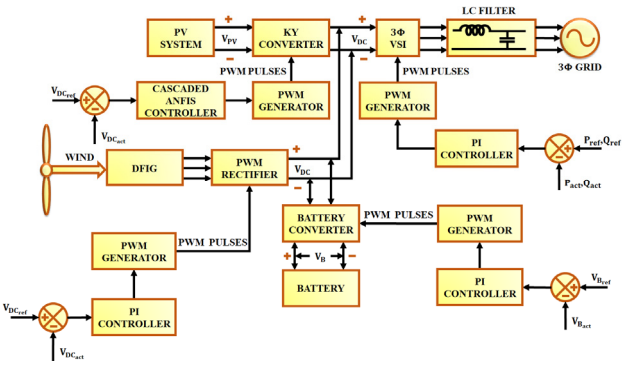

Fig. 1. Proposed hybrid energy based microgrid

The error obtained by analogising the actual DC voltage $V_{DC_{act}}$ of the PWM rectifier with the reference voltage $V_{DC_{ref}}$ is supplied to the PI controller. The control signal generated by the PI controller is supplied into the PWM generator for the generation of PWM pulses. These pulses control the switching operation of the rectifier so as to generate a controlled DC output. The

error signal produced by comparing the actual DC voltage output $V_{B_{act}}$ of the battery with the reference voltage $V_{B_{ref}}$ is provided to the PI controller. The controller generates a control signal, which is fed to the PWM generator for generating PWM pulses. These pulses control the switching operation of the battery converter for providing a constant DC supply. The 3φ VSI, which converts the DC output voltage of the converter into AC voltage, is connected to the 3φ grid through an LC filter.

Proposed system modelling.

a) Solar PV modeling. The solar cell is the most essential component of a PV system that generates DC voltage when exposed to sun light based on the phenomenon of PV effect. A PV panel consists of many solar cells, which are linked in parallel and series, with the parallel connection expansion increasing the current and the series connection expansion increasing the voltage. A PV array is made up of many PV panels. Figure 2 illustrates the equivalent circuit of a PV cell.

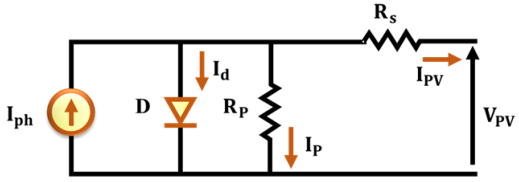

Fig. 2. Equivalent circuit of PV cell

By applying Kirchchoff's current law

$$I_{PV} = I_{ph} - I_d - I_P, \tag{1}$$

where

$$I_d = I_o \cdot \left[\exp\left(\frac{V_{PV} + I_{PV} \cdot R_S}{n \cdot v} \right) - 1 \right], \tag{2}$$

$$I_p = \left(\frac{V_{PV} + I_{PV} \cdot R_S}{R_P} \right), \tag{3}$$

$$I_{PV} = I_{ph} - I_o \cdot \left[\exp\left(\frac{V_{PV} + I_{PV} \cdot R_S}{n \cdot v} \right) - 1 \right] - \frac{V_{PV} + I_{PV} \cdot R_S}{R_P}, \tag{4}$$

where I_{PV} is the PV output current that flows through the series resistance R_S; V_{PV} is the PV output voltage; I_{ph} is the photo generated current; I_d is the diode saturation current; I_o is the reverse saturation current; I_P is the current that flows through the shunt resistance R_P; n is the number of series connected solar PV cells; v is the junction thermal voltage; a is the diode ideality constant; q is the electron charge ($1.602 \cdot 10^{-19}$ C); k is the Boltzmann constant ($1.381 \cdot 10^{-23}$ J/K); T is the temperature of p-n junction.

The PV panel's open circuit voltage is:

$$V_{OC} = \frac{a \cdot k \cdot T}{q} \log_n \left(\frac{I_{ph}}{I_d} + 1 \right). \tag{5}$$

b) KY converter. KY converter is a voltage boosting converter, which has low output voltage ripple. This converter has the same properties as that of the buck converter and has rapid transient load response. It comprises of two power switches S_1 and S_2, a diode VD, an output capacitor C, an energy transferring capacitor C_b, an output inductor L and a load resistance R. The terms v_o and v_{pv} represent the output and input voltage respectively. The i_{pv} specifies the input current and i denotes the current flowing through L. The voltage across C_b is denoted as v_{pv} as the voltage across C_b completely follows the input voltage v_{pv}. Figure 3 presents the equivalent structure of KY converter. The two different modes of operation of KY converter are illustrated in Fig. 4.

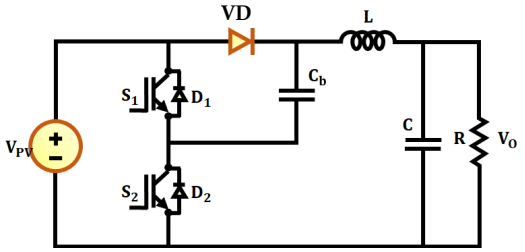

Fig. 3. Circuit diagram of KY converter

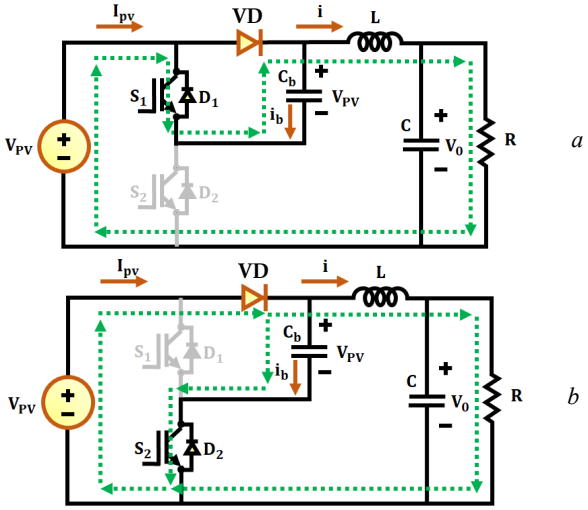

Fig. 4. KY converter operating modes: *a*) mode 1; *b*) mode 2

Mode 1. At this stage, the power switch S_1 is switched ON, whereas the power switch S_2 is switched OFF. On subtracing the output voltage v_o from the sum of voltage v_{pv} across C_b and input voltage v_{pv}, the magnitude of voltage across the inductor L is determined. The inductor L is magnetized in this mode. As a result, the differential equations are:

$$L \cdot \frac{\partial i}{\partial t} = 2 \cdot v_{pv} - v_o; \quad C \cdot \frac{\partial v_o}{\partial t} = i - \frac{v_o}{R}; \quad i_{PV} = i. \tag{6}$$

Mode 2. At this stage, the power switch S_1 is switched OFF, whereas the power switch S_2 is switched ON. During this mode, the demagnetisation of inductor L takes place. On subtracing the output voltage v_o from voltage v_{pv} across C_b, the magnitude of voltage across the inductor L is determined. As a result, the differential equations are:

$$L \cdot \frac{\partial i}{\partial t} = v_{pv} - v_o; \quad C \cdot \frac{\partial v_o}{\partial t} = i - \frac{v_o}{R}; \quad i_{PV} = i + i_b. \tag{7}$$

where i_b is the current of energy transferring capacitor.

The relationship between v_{pv} and v_o is represented as follows:

$$\frac{v_o}{v_{pv}} = 1 + D, \tag{8}$$

where D is the duty cycle.

The intermittent nature of the solar energy has a huge impact on the KY converter output, so it fluctuates and remains unstable. The operation of the converter is made more efficient by using cascaded ANFIS controller.

c) ANFIS controller. ANFIS is a versatile intelligent control technique, which is first introduced by Jang in the year 1993, combines both the ANN and fuzzy inference system (FIS).To deal with non-linear functions, a system is transformed into if-then rules using ANFIS. The structure of ANFIS controller comprises of five different layers, which are fuzzification layer, rule layer, normalization layer, defuzzification layer and output layer as represented in Fig. 5. Here, the two inputs to the ANFIS structure are *a* and *b*, while the output is *f*.

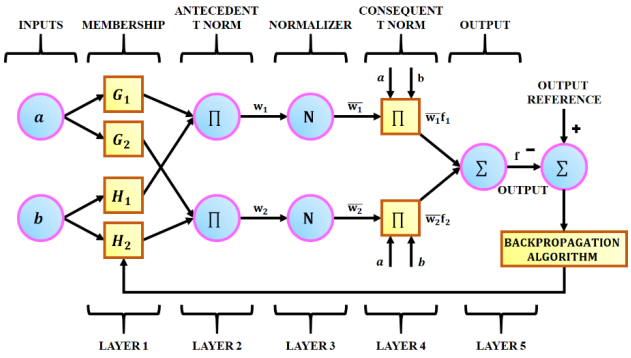

Fig. 5. ANFIS structure

The Sugeno FIS-based ANFIS if-then rule configuration is as follows:

rule 1: if *a* is G_1 and *b* is H_1; then $f_1 = p_1 \cdot a + q_1 \cdot b + r_1$;

rule 2: if *a* is G_2 and *b* is H_2; then $f_2 = p_2 \cdot a + q_2 \cdot b + r_2$;

The design parameters for training process are p_i, q_i and r_i, where i = 1, 2. The fuzzy sets are represented by the terms G_1 and H_1.

In the initial layer, the membership functions for each of the specified input data are developed. The membership functions of the adaptive nodes of this layer are given by:

$$O_{1,i} = \mu_{Gi}(a),\ i = 1,2; \tag{9}$$

$$O_{1,i} = \mu_{Hj}(b),\ i = 1,2; \tag{10}$$

where the membership grades for fuzzy set (G_1, G_2, H_1 and H_2) are represented as $\mu_{Gi}(a)$ and $\mu_{Hj}(b)$.

The second layer consists of circular nodes that are labeled as π. This layer multiplies the input signals as shown in the following mathematical expression

$$O_{2,i} = w_i = \mu_{Gi}(a) \times \mu_{Hj}(b),\ i = 1,2; \tag{11}$$

where the term w_i specifies the firing strength of node *i*.

The third layer is the normalization layer, which consists of circular nodes that are labeled as *N*. The output of the second layer is normalised in this layer, as given below:

$$O_{3,i} = \overline{w}_l = \frac{w_i}{w_1 + w_2},\quad i = 1, 2, \tag{12}$$

where $\overline{w}_l$ specifies the normalized firing strengths.

The third layer output is simplified in the fourth layer and the result is given by:

$$O_{4,i} = \overline{w}_l \cdot f_i = \overline{w}_l \cdot \left(p_i \cdot g + q_i + r_i\right),\quad i = 1, 2, \tag{13}$$

where $\{p_i, q_i, r_i\}$ represents the parameter set and the term $\overline{w}_l$ specifies the output of the third layer.

The summing of all the inputs is carried out in the final layer. This layer consists of only one node, which is labeled as Σ. The overall result is given as:

$$O_{5,i} = \sum_{i=1}^{2} \overline{w}_l \cdot f_i = \frac{w_1 \cdot f_1 + w_2 \cdot f_2}{w_1 + w_2}. \tag{14}$$

The parameters of first and fourth layer are known as premise and consequent parameters, respectively. The first layer parameters are tuned by back propagation approach, while the fourth layer parameters are tuned by least square approach. These two approaches improve the system's accuracy and speed of convergence, hence the learning ability of ANFIS is better.

d) Cascaded ANFIS controller. The conventional ANFIS method has certain limitations like computational complexity and the curse of dimensionality. These limitations are overcome by using cascaded ANFIS method, which is an extension of conventional ANFIS. It comprises of two important modules namely, pair selection module and training module. The flow chart of cascaded ANFIS is represented in Fig. 6,*a*.

Pair selection module. The overall procedure of the pair selection module is illustrated in Fig. 6,*b*. Here, ANFIS structure with two inputs and one output is used to find the best matching pair from the input variables. In this module, sequential feature selection process is carried out and the matching pair is obtained as the final outcome. To go through all two pair combinations, a nested loop is used. The term NI in Fig. 6,*b* specifies the number of input variables. The chosen inputs for the system are $input_i$ and $input_j$. The value of root mean square error (RMSE), which is represented as E_p is computed and saved for comparing with the prior value of RMSE (E_{prev}). The matching pair is extracted by checking the lowest RMSE value at the conclusion of second loop. The training phase begins after the pairs have been chosen.

Train model module. The train model module also uses the ANFIS model with two inputs similar to the pair selection module. It receives the matching pairs from the pair selection module as input, and outputs are produced for each set of inputs provided. When the target error is reached, the process is completed; otherwise, the next iteration is performed. The operational flowchart of training module is presented in Fig. 7.

Consider X_1, X_2, X_3 and X_4 as the input variables of optimization problem:

$$\text{Input} = \{X_1, X_2, X_3, X_4\}. \tag{15}$$

The four input variables form pairs with the best match in the pair selection module as specified below:

$$Input_{pairs} = \{X_1, X_3\}, \{X_2, X_1\}, \{X_3, X_4\}, \{X_4, X_1\}. \tag{16}$$

For each input pair, ANFIS model with two inputs are used to generate two outputs namely, $RMSE_i$ and Y_i:

$$RMSE = \sqrt{\overline{(A-P)^2}}\ ; \tag{17}$$

$$RMSE_{A,P} = \left[\sum_{i=1}^{N} \frac{(O_{Ai} - O_{Pi})^2}{N}\right]^{\frac{1}{2}}, \tag{18}$$

where the actual results and predicted results are specified as *A* and *P*, respectively; *N* is the sample size.

The output *f* is:

$$f = \frac{w_1}{w_1 + w_2} \cdot f_1 + \frac{w_2}{w_1 + w_2} \cdot f_2 + \frac{w_3}{w_2 + w_3} \cdot f_3 + \frac{w_4}{w_3 + w_4} \cdot f_4 . \tag{19}$$

The initial iteration comes to an end after the determination of *RMSE* and *Y*. The *RMSE* and goal error are compared before moving on to the next iteration. The outputs obtained from the first iteration are Y_1, Y_2, Y_3 and Y_4, which are used as inputs for the second iteration.

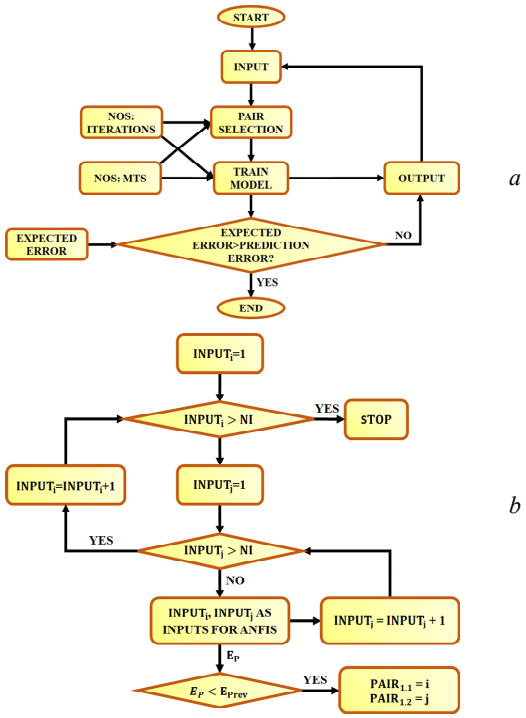

Fig 6. Flow chart of cascaded ANFIS (*a*) and pair selection module (*b*)

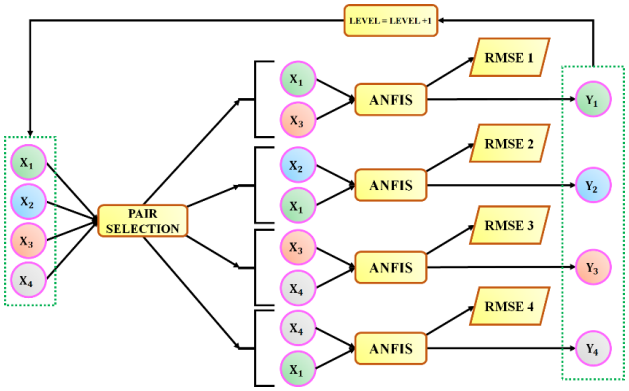

Fig. 7. Structure of training module

e). Grid voltage synchronization using PI controller. Voltage control and current control are the two different types of control techniques adopted for controlling the 3φ VSI. In case of voltage controlled VSI, the phase angle between grid voltage and the inverter voltage output is used to establish power flow control, where as in case current controlled VSI, the reactive and active components of the injected current to the grid are controlled by the use of PWM approach. The current control technique provides quick response and is less sensitive to grid voltage distortion and voltage phase shifts. The voltage control technique is sensitive to small phase errors and when the grid voltage is distorted, significant harmonic currents occur. As a result, the current control technique is highly preferred for controlling the operation of grid connected inverter. Among different current control techniques, the PI controller is widely adopted approach for compensating current errors as it provides quick steady state response, minimum current ripple and stable switching frequency. Figure 8 illustrates the process of grid voltage synchronization using PI controller.

The PI controller minimizes the error, which is determined by comparing the actual output current of the inverter with the reference grid current. The proportional

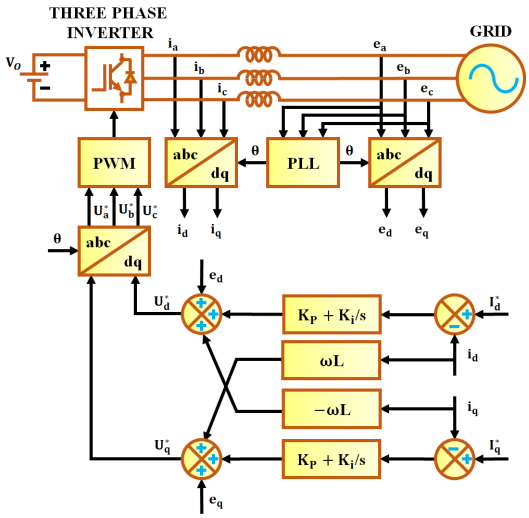

Fig. 8. A synchronous PI controller-based grid voltage synchronization

constant K_P and the integral constant K_I are the two different parameters that are involved in the calculation procedure of the controller. Here both proportional and integral operation takes place. In case of proportional operation, the error e is multiplied with the gain K_P, whereas in case of integral operation, the error e is integrated and then multiplied with gain K_I. At the end of both operations, the steady state error is totally minimized and the reference signal is generated in a short span of time. This controller is capable of working with both stationary reference frame (αβ) and synchronous reference frame (dq). Here the PI controller is used in dq reference frame for achieving effective grid voltage synchronization.

The grid-connected inverter's output voltage in the synchronous (dq) frame is calculated using the inverter's mathematical model, as shown below:

$$\begin{bmatrix} u_d \\ u_q \end{bmatrix} = L \cdot \frac{\mathrm{d}}{\mathrm{d}t}\begin{bmatrix} i_d \\ i_q \end{bmatrix} + R \cdot \begin{bmatrix} i_d \\ i_q \end{bmatrix} + \omega \cdot L \cdot \begin{bmatrix} -i_q \\ i_d \end{bmatrix} + \begin{bmatrix} e_d \\ e_q \end{bmatrix}, \quad (20)$$

where u_d and u_q are the Park transformation components of the inverter output; e_d and e_q are the Park transformation components of the grid voltage; R, L are the resistance and inductance between the grid and the grid connected inverter, respectively; ω is the angular frequency of the grid.

The structure of synchronous PI controller for grid tied inverter is illustrated in Fig. 8. The current vector components indicated in the synchronous reference frame (dq) are compensated using two PI controllers One PI controller compares I_d and I_d^*, while the other compares I_q and I_q^* and generate errors that are minimized to zero. The power factor and output power are regulated by varying the q-axis and d-axis currents.

f) DFIG based WECS. The wind turbine produces mechanical energy by conversion of the kinetic energy of the wind. The developed mechanical power is:

$$P_m = \frac{1}{2} \cdot C_p(\lambda, \beta) \cdot \pi \cdot r^2 \cdot \rho \cdot V_w^3, \quad (21)$$

where C_p is the power coefficient; λ is the tip speed ratio; β is the pitch angle; r is the radius of wind turbine, m; ρ is the air density, kg/m^3; V_w is the wind speed, m/s.

Figure 9 illustrates the direct interfacing of the stator to the grid, while a grid-side converter (GSC) and rotor-

side converter (RSC) are used for interfacing the rotor to the grid. The control of DC link voltage in between the two converters is performed by the GSC. The reactive power required by DFIG for magnetization is provided by RSC. A PWM rectifier converts the AC voltage generated by the DFIG to DC voltage. An error signal is produced when the actual DC voltage $V_{DC_{act}}$ of the PWM rectifier is compared to the reference voltage $V_{DC_{ref}}$. The error thus obtained is given as input to the PI controller. In the PI controller, proportional and integral action takes place and the error is eliminated. The PWM generator receives the control signal generated by the PI controller and generates PWM pulses. The switching operation of the rectifier is monitored using these pulses in order to generate a steady and controlled DC output voltage V_{DC}.

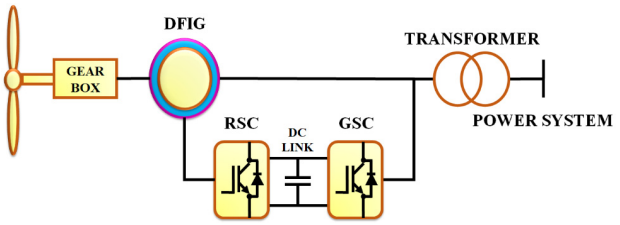

Fig. 9. DFIG based WECS

g) PI controller based BESS. The actual battery voltage $V_{B_{act}}$ and the reference voltage $V_{B_{ref}}$ are compared to find the steady state error *e*. This error is fed into the PI controller, which performs both proportional and integral control operations and generates the control signal *u* as shown below:

$$u = K_P \cdot e + K_I \cdot \int e dt \,. \qquad (22)$$

The circuit diagram of PI controller based BESS is illustrated in Fig. 10. The PWM generator generates PWM pulses based on the control signal, which is obtained from the PI controller. The resultant PWM pulses controls the duty cycle of the battery converter in order to enable buck as well as boost mode of operation. The battery is charged during the buck mode of operation and discharged during the boost mode of operation.

Results and discussions. A hybrid energy based microgrid is designed with PV, WECS and BESS for getting a reliable power supply in this work. By adopting cascaded ANFIS controller and PI controllers the overall system voltage stability is maintained. The performance of the proposed hybrid energy based microgrid is analysed by using MATLAB simulation and the results are obtained as specified below. The specifications of the solar panel, WECS, converters, BESS and load are mentioned in Table 1.

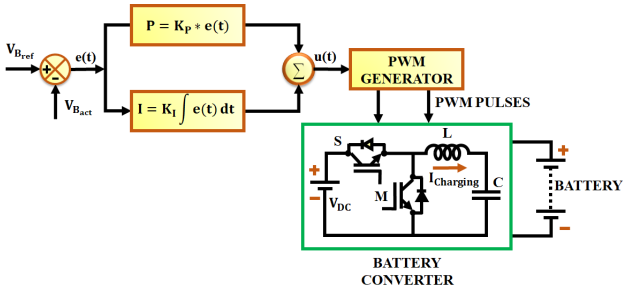

Fig. 10. PI controller for BESS

Table 1

Solar panel, WECS, KY converter, BESS, battery converter and load specifications

PV Panel	
Parameters	Ratings
Peak power	10 kW
No. of solar PV panels	750 W, 13 panels
Short circuit voltage V_{SC}	12 V
Short circuit current I_{SC}	62.5 A
Open circuit voltage V_{OC}	22.6 V
No. of series connected solar cells	36
WECS	
No. of wind turbines	1
Power	10 kW
Voltage	575 V
Speed range	4–16 m/s
KY converter	
L	4 mH
C_b	22 μF
C	1000 μF
Switching frequency	10 kHz
BESS	
Capacity	100 A·h
No. of battery units	5.12 V
Battery converter	
L	1 mH
C	1000 μF
Switching frequency	10 kHz
Load	
Capacity	5 kW

The waveforms that indicate the magnitude of voltage and current obtained from the PV panel is illustrated in Fig. 11. The panel voltage experiences a slight rise at 0.2 s and maintained constant, while the PV panel output current is constantly maintained at 25 A after 0.1 s. However, the effects of the variations in operating condition are seen on the panel output current, which also happens to be the converter's input.

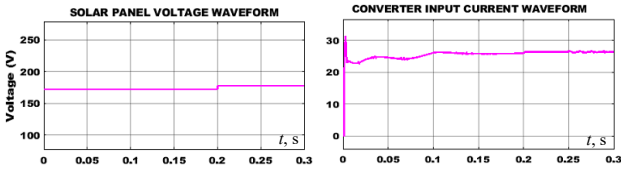

a *b*

Fig. 11. Solar panel: output voltage (*a*); output current (*b*)

The KY converter output voltage and current settles quickly after undergoing incessant fluctuations at 0.15 s and 0.1 s respectively due to the application of cascaded fuzzy controller as illustrated in Fig. 12. Thus, the adopted cascaded fuzzy assisted KY converter displays a remarkable performance in stabilizing and enhancing the PV output within a short period of time.

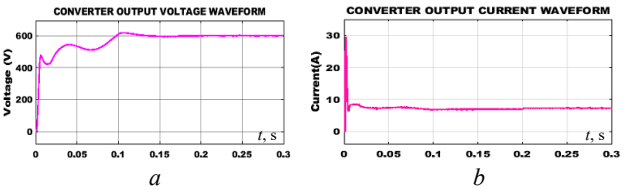

a *b*

Fig. 12. KY converter:
output voltage (*a*); output current waveform (*b*)

In Fig. 13,*a* the output voltage of the DFIG is around 550 V with slight fluctuations owing to the wind energy intermittency. The output voltage of the PWM rectifier undergoes a sudden rise at the beginning and gradually settles down at 0.15 s with the implementation of PI controller as seen in Fig. 13,*b*. The output of the PI controller based PWM rectifier is constant and remains distortion free.

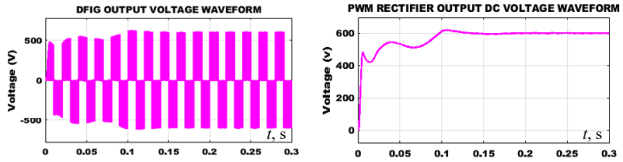

a *b*

Fig. 13. Output voltage waveform of DFIG (*a*) and PWM rectifier (*b*)

The battery voltage and current waveforms are illustrated in Fig. 14,*a* and Fig. 14,*b* respectively. The SOC of the battery is about 60 % as indicated in Fig. 14,*c*. When the SOC of the battery is below 60 %, the battery converter executes battery charging by operating in buck mode. When the SOC of the battery is above 60 %, the battery converter executes battery discharging by operating in boost mode. From the figure, it is evident that the battery voltage and current initially suffers from fluctuations and becomes stable within a short period due to the application of PI controller.

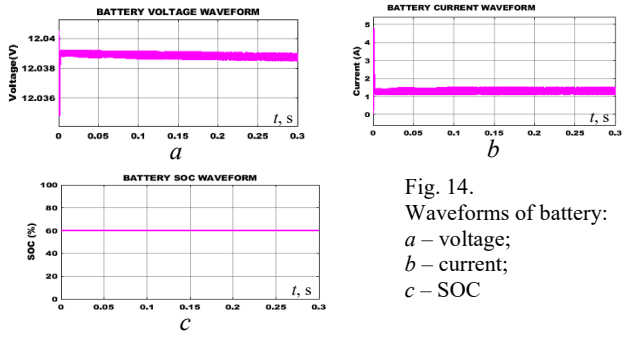

a *b* *c*

Fig. 14. Waveforms of battery: *a* – voltage; *b* – current; *c* – SOC

Figure 15 presents the waveforms that indicate the magnitude of the real and reactive power. The magnitude of reactive power gradually increases and becomes stable at a value of 5400 W at 0.03 s. The magnitude of reactive power is –50 VAr from 0.1 s.

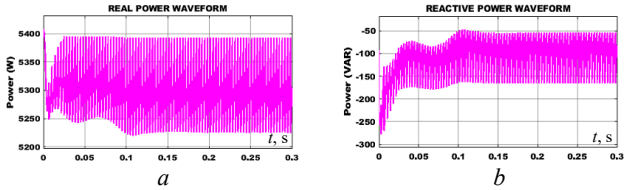

a *b*

Fig. 15.Waveforms of real power (*a*) and reactive power (*b*)

The waveforms that represent the grid voltage and current are seen in Fig. 16. Both the grid voltage and grid current are stable without fluctuations with the effective grid voltage synchronization achieved by PI controller. The magnitude of grid voltage is maintained at 230 V and the magnitude of grid current is maintained at 10 A.

The voltage gain and efficiency of different DC-DC converters are compared with KY converter in Fig. 17,*a* and Fig. 17,*b* respectively. From Fig. 17,*a*, it is clear that the voltage gain of KY converter is 1:10 and it is comparatively higher than the other four conventional DC-DC converters. The efficiency of cascaded ANFIS controller assisted KY converter is about 93 %, which is higher than the efficiency of other 4 conventional DC-DC converters as represented in Fig. 17,*b*.

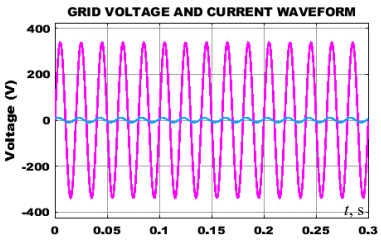

Fig. 16. Waveform of grid voltage and current

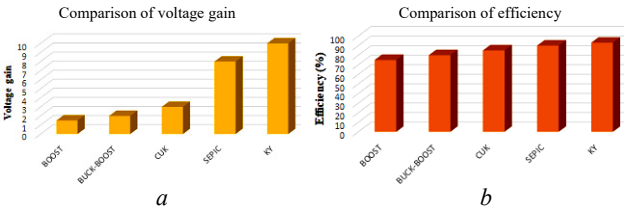

a *b*

Fig. 17. Comparison of voltage gain (*a*) and efficiency (*b*) of various DC-DC converters

Hardware implementation is represented in Fig. 18. In Fig. 19, 20 the oscillograms of voltages for KY converter, which got from experiments, are shown.

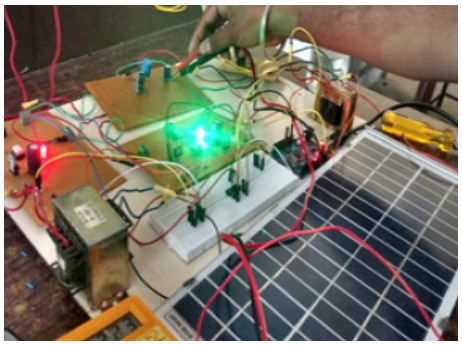

Fig. 18. Hardware setup

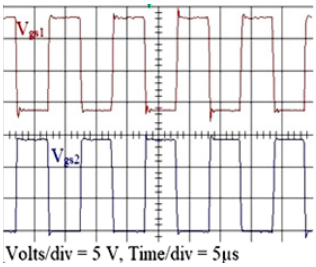

Fig. 19. Gating pulses of S1 and S2

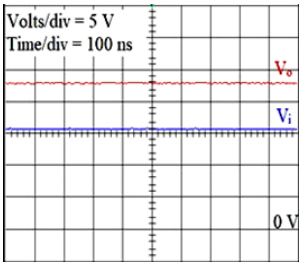

Fig. 20. V_o and V_i of KY converter

Conclusions.

A hybrid energy based microgrid that combines renewable energy sources like photovoltaic system and wind energy conversion system is designed for the purpose of heightening the overall system stability and reliability. The KY converter, which is connected to the output side of the photovoltaic system, enhances its output voltage with reduced switching loss. The operation of the converter is optimized with the assistance of cascaded adaptive neuro fuzzy interface system controller. A proportional integral controller is used to stabilize the output of the doubly fed induction generator based wind energy conversion system. The battery energy storage system, which is interfaced with

the microgrid through a battery converter, ensures consistent supply of power. The state of charge of the battery is monitored and controlled with the help of a proportional integral controller. The adopted control approach of cascaded adaptive neuro fuzzy interface system assisted KY converter operates with an impressive efficiency of 93 %.

Conflict of interest. The authors declare that they have no conflicts of interest

REFERENCES

1. Mosaad M.I., Ramadan H.S.M., Aljohani M., El-Naggar M.F., Ghoneim S.S.M. Near-Optimal PI Controllers of STATCOM for Efficient Hybrid Renewable Power System. *IEEE Access*, 2021, vol. 9, pp. 34119-34130. doi: https://doi.org/10.1109/ACCESS.2021.3058081.

2. Ali Moussa M., Derrouazin A., Latroch M., Aillerie M. A hybrid renewable energy production system using a smart controller based on fuzzy logic. *Electrical Engineering & Electromechanics*, 2022, no. 3, pp. 46-50. doi: https://doi.org/10.20998/2074-272X.2022.3.07.

3. Kumar D., Zare F., Ghosh A. DC Microgrid Technology: System Architectures, AC Grid Interfaces, Grounding Schemes, Power Quality, Communication Networks, Applications, and Standardizations Aspects. *IEEE Access*, 2017, vol. 5, pp. 12230-12256. doi: https://doi.org/10.1109/ACCESS.2017.2705914.

4. Farrokhabadi M., Konig S., Canizares C.A., Bhattacharya K., Leibfried T. Battery Energy Storage System Models for Microgrid Stability Analysis and Dynamic Simulation. *IEEE Transactions on Power Systems*, 2018, vol. 33, no. 2, pp. 2301-2312. doi: https://doi.org/10.1109/TPWRS.2017.2740163.

5. Lotfi H., Khodaei A. AC Versus DC Microgrid Planning. *IEEE Transactions on Smart Grid*, 2017, vol. 8, no. 1, pp. 296-304. doi: https://doi.org/10.1109/TSG.2015.2457910.

6. Praveen Kumar T., Ganapathy S., Manikandan M. Improvement of voltage stability for grid connected solar photovoltaic systems using static synchronous compensator with recurrent neural network. *Electrical Engineering & Electromechanics*, 2022, no. 2, pp. 69-77. doi: https://doi.org/10.20998/2074-272X.2022.2.10.

7. Errouissi R., Al-Durra A., Muyeen S.M. A Robust Continuous-Time MPC of a DC–DC Boost Converter Interfaced With a Grid-Connected Photovoltaic System. *IEEE Journal of Photovoltaics*, 2016, vol. 6, no. 6, pp. 1619-1629. doi: https://doi.org/10.1109/JPHOTOV.2016.2598271.

8. Jedari Zare Zadeh M., Fathi S.H. A New Approach for Photovoltaic Arrays Modeling and Maximum Power Point Estimation in Real Operating Conditions. *IEEE Transactions on Industrial Electronics*, 2017, vol. 64, no. 12, pp. 9334-9343. doi: https://doi.org/10.1109/TIE.2017.2711571.

9. De Morais J.C. dos S., De Morais J.L. dos S., Gules R. Photovoltaic AC Module Based on a Cuk Converter With a Switched-Inductor Structure. *IEEE Transactions on Industrial Electronics*, 2019, vol. 66, no. 5, pp. 3881-3890. doi: https://doi.org/10.1109/TIE.2018.2856202.

10. Tey K.S., Mekhilef S., Seyedmahmoudian M., Horan B., Oo A.T., Stojcevski A. Improved Differential Evolution-Based MPPT Algorithm Using SEPIC for PV Systems Under Partial Shading Conditions and Load Variation. *IEEE Transactions on Industrial Informatics*, 2018, vol. 14, no. 10, pp. 4322-4333. doi: https://doi.org/10.1109/TII.2018.2793210.

11. Tey K.S., Mekhilef S. Modified Incremental Conductance Algorithm for Photovoltaic System Under Partial Shading Conditions and Load Variation. *IEEE Transactions on Industrial Electronics*, 2014, vol. 61, no. 10, pp. 5384-5392. doi: https://doi.org/10.1109/TIE.2014.2304921.

12. Ali M.S., Wang L., Alquhayz H., Rehman O.U., Chen G. Performance Improvement of Three-Phase Boost Power Factor Correction Rectifier Through Combined Parameters Optimization of Proportional-Integral and Repetitive Controller. *IEEE Access*, 2021, vol. 9, pp. 58893-58909. doi: https://doi.org/10.1109/ACCESS.2021.3073004.

13. Seidi Khorramabadi S., Bakhshai A. Critic-Based Self-Tuning PI Structure for Active and Reactive Power Control of VSCs in Microgrid Systems. *IEEE Transactions on Smart Grid*, 2015, vol. 6, no. 1, pp. 92–103. doi: https://doi.org/10.1109/TSG.2014.2354651.

14. Ali M., Tariq M., Lodi K.A., Chakrabortty R.K., Ryan M.J., Alamri B., Bharatiraja C. Robust ANN-Based Control of Modified PUC-5 Inverter for Solar PV Applications. *IEEE Transactions on Industry Applications*, 2021, vol. 57, no. 4, pp. 3863-3876. doi: https://doi.org/10.1109/TIA.2021.3076032.

15. Hannan M.A., Ghani Z.A., Hoque M.M., Ker P.J., Hussain A., Mohamed A. Fuzzy Logic Inverter Controller in Photovoltaic Applications: Issues and Recommendations. *IEEE Access*, 2019, vol. 7, pp. 24934-24955. doi: https://doi.org/10.1109/ACCESS.2019.2899610.

16. Garcia P., Garcia C.A., Fernandez L.M., Llorens F., Jurado F. ANFIS-Based Control of a Grid-Connected Hybrid System Integrating Renewable Energies, Hydrogen and Batteries. *IEEE Transactions on Industrial Informatics*, 2014, vol. 10, no. 2, pp. 1107-1117. doi: https://doi.org/10.1109/TII.2013.2290069.

17. Puchalapalli S., Tiwari S.K., Singh B., Goel P.K. A Microgrid Based on Wind-Driven DFIG, DG, and Solar PV Array for Optimal Fuel Consumption. *IEEE Transactions on Industry Applications*, 2020, vol. 56, no. 5, pp. 4689-4699. doi: https://doi.org/10.1109/TIA.2020.2999563.

18. Byrne R.H., Nguyen T.A., Copp D.A., Chalamala B.R., Gyuk I. Energy Management and Optimization Methods for Grid Energy Storage Systems. *IEEE Access*, 2018, vol. 6, pp. 13231-13260. doi: https://doi.org/10.1109/ACCESS.2017.2741578.

19. Li X., Wang S. Energy management and operational control methods for grid battery energy storage systems. *CSEE Journal of Power and Energy Systems*, 2021, vol. 7, no. 5, pp. 1026-1040. doi: https://doi.org/10.17775/CSEEJPES.2019.00160.

20. Fan F., Kockar I., Xu H., Li J. Scheduling framework using dynamic optimal power flow for battery energy storage systems. *CSEE Journal of Power and Energy Systems*, 2022, vol. 8, no. 1, pp. 271-280. doi: https://doi.org/10.17775/CSEEJPES.2020.03710.

21. Gangatharan S., Rengasamy M., Elavarasan R.M., Das N., Hossain E., Sundaram V.M. A Novel Battery Supported Energy Management System for the Effective Handling of Feeble Power in Hybrid Microgrid Environment. *IEEE Access*, 2020, vol. 8, pp. 217391-217415. doi: https://doi.org/10.1109/ACCESS.2020.3039403.

Received 07.06.2022
Accepted 23.08.2022
Published 06.01.2023

Chindam Sathish[1], *Research Scholar*,
Ilanji Akilandam Chidambaram[1], *Professor,*
Mani Manikandan[2], *Professor,*
[1] Annamalai University,
Chidambaram, Tamil Nadu, 608002, India,
e-mail: chindam.satish@jits.ac.in (Corresponding Author);
driacdm@gmail.com
[2] Jyothishmathi Institute of Technology and Science,
Karimnagar, Telangana, 505481, India,
e-mail: cm.manikandan@gmail.com

How to cite this article:
Sathish Ch., Chidambaram I.A., Manikandan M. Intelligent cascaded adaptive neuro fuzzy interface system controller fed KY converter for hybrid energy based microgrid applications. *Electrical Engineering & Electromechanics*, 2023, no. 1, pp. 63-70. doi: https://doi.org/10.20998/2074-272X.2023.1.09